Toughening of Polyamide 6 with a Maleic Anhydride Functionalized Acrylonitrile–Butadiene–Styrene Copolymer

X. Y. Xu,[1] S. L. Sun,[1] Z. C. Chen,[1] H. X. Zhang[1,2]

[1]*Institute of Chemical Engineering, Changchun University of Technology, Changchun 130012, China*
[2]*Changchun Institute of Applied Chemistry, Graduate School, Chinese Academy of Sciences, Changchun 130022, China*

Received 10 August 2006; accepted 4 September 2007
DOI 10.1002/app.28238
Published online 9 May 2008 in Wiley InterScience (www.interscience.wiley.com).

ABSTRACT: Maleic anhydride functionalized acrylonitrile–butadiene–styrene (ABS-*g*-MA) copolymers were prepared via an emulsion polymerization process. The ABS-*g*-MA copolymers were used to toughen polyamide 6 (PA-6). Fourier transform infrared results show that the maleic anhydride (MA) grafted onto the polybutadiene phase of acrylonitrile–butadiene–styrene (ABS). Rheological testing identified chemical reactions between PA-6 and ABS-*g*-MA. Transmission electron microscopy and scanning electron microscopy displayed the compatibilization reactions between MA of ABS-*g*-MA and the amine and/or amide groups of PA-6 chain ends, which improved the disperse morphology of the ABS-*g*-MA copolymers in the PA-6 matrix. The blends compatibilized with ABS-*g*-MA exhibited notched impact strengths of more than 900 J/m. A 1 wt % concentration of MA in ABS-*g*-MA appeared sufficient to improve the impact properties and decreased the brittle–ductile transition temperature from 50 to 10°C. Scanning electron microscopy results show that the shear yielding of the PA-6 matrix was the major toughening mechanism. © 2008 Wiley Periodicals, Inc. J Appl Polym Sci 109: 2482–2490, 2008

Key words: compatibility; emulsion polymerization; polyamides; toughness

INTRODUCTION

Commercial polyamides, such as polyamide 6 (PA-6), are crystalline engineering thermoplastics that exhibit high performance characteristics, such as a high melting point, high mechanical strength, stiffness, and excellent resistance to solvents, fatigue, and abrasion; however, many drawbacks remain to be improved, such as brittleness with notching, high moisture absorption, poor dimensional stability, and marginal heat deflection temperatures.[1,2] To improve the notch impact toughness, many suitable elastomers have been used to toughen polyamides, such as functionalized hydrocarbon elastomers[3–10] and core–shell impact modifiers.[11–13] A major distinction between core–shell particles and other types of impact modifiers is that the size of core–shell particles is set during the synthesis process.[14]

In polyamides, the amide groups impart a strong hydrogen bonding capability.[15] Because of the highly polar and hydrogen-bonded structure of the backbone, as a general rule, polyamides are immiscible with most commercially known polymers. In addition, the high interfacial tension between polyamides and other polymers leads to highly phase-separated blends. Fortunately, the inherent chemical functionality of polyamides makes them an attractive candidate for modification. To improve the miscibility of blends and increase the interfacial adhesion between the matrix and the disperse phase, the method of reactive compatibilization has often been used to obtain blends with desirable properties; this method uses a block or graft copolymer *in situ* as a compatibilizer during melt-blending via a chemical reaction of the functionalized polymeric components and the matrix at the interface.[16–20]

Blends of PA-6 and acrylonitrile–butadiene–styrene (ABS) core–shell particles are of significant commercial interest; however, the simple blending of PA-6 and ABS generally results in poor mechanical properties and often requires compatibilization. Various approaches to the reactive compatibilization of PA-6/ABS have been reported in the literature.[21–24] The preferential compatibilization strategy is to incorporate a functional copolymer that is capable of reacting with the amine and/or amide groups of the PA-6 and that is miscible with the styrene-acryloni-

Correspondence to: H. X. Zhang (zhanghx@mail.ccut.edu.cn).

Contract grant sponsor: Jilin Provincial Science and Technology Department; contract grant number: 20060501.
Contract grant sponsor: Jilin Province Educational Department; contract grant number: 200634.
Contract grant sponsor: Natural Science Foundation of Changchun University of Technology.

TABLE I
Properties of ABS and ABS-*g*-MA

Designation	Rubber content (wt %)	AN/St (wt/wt)	MA (wt %)	ABS particle size (μm)	Torque (Nm)[a]
ABS	60	25/75	0	342	23.4
ABS-*g*-MA (0.5%)	60	25/75	0.5	351	23.7
ABS-*g*-MA (1%)	60	25/75	1	348	23.2
ABS-*g*-MA (3%)	60	25/75	3	356	23.6

[a] The measurements were taken at 240°C and 50 rpm after 6 min.

trile copolymer (SAN) phase of ABS. This copolymer decreases the interfacial tension and improves interfacial adhesion between the two phases; this is beneficial to the dispersion of the ABS phase. Patents[25–27] have described the use of a terpolymer of styrene (St), acrylonitrile (AN), and maleic anhydride (MA) as a compatibilizer for PA-6/ABS blends. St and MA copolymers have also been used as compatibilizers for PA-6/ABS blends because they are miscible with SAN copolymers and can react with the PA-6 matrix.[28–30] Majumdar and coworkers[21–23] used a series of imidized acrylic copolymer and St–AN–MA terpolymers as compatibilizers for PA-6/ABS blends over a range of compatibilizer contents. These imidized acrylic materials were miscible with SAN and contained acid anhydride functionalities capable of reacting with the amine end groups of polyamides. Recently, epoxy-functionalized copolymers, such as glycidyl methacrylate/methyl methacrylate copolymer, were synthesized as compatibilizers of PA-6/ABS blends.[31,32] Sun et al.[24] investigated the use of epoxy-functionalized ABS core–shell particles via an emulsion polymerization process as compatibilizers of PA-6/ABS blends.

In this study, maleic anhydride functionalized acrylonitrile–butadiene–styrene (ABS-*g*-MA) was prepared in an emulsion polymerization process. During the synthesis of ABS, different contents of MA monomer were added to the reactive system. Compared with PA-6/compatibilizer/ABS blends, the functionalization of the impact modifier was carried out during the preparation process of ABS, so this method was simpler. The focus of this study was to explore the effect of MA content in the ABS-*g*-MA copolymer on the rheological, morphological, and mechanical properties of the PA-6 blends. Scanning electron microscopy (SEM) was used to observe the fracture morphology of the toughened PA-6, and the toughening mechanisms were then proposed.

EXPERIMENTAL

Materials

PA-6 was purchased from Longjiang Plastics Plant (Heilongjiang, China). The concentrations of the carboxyl and amine groups were 42.6 and 51.2 μequiv/g, respectively. Its intrinsic viscosity was 2.5 dL/g (0.01 g/mL, formic acid solution, 30°C), and its number-average molecular weight was 2.4×10^4 g/mol. The ABS and ABS-*g*-MA materials were synthesized by the emulsion polymerization method in our laboratory. Table I describes the ABS and ABS-*g*-MA materials used in this study. The particle sizes of these materials were determined with a Brookhaven particle size analyzer (Holtsville, NY). The measuring technique imagines a detector of light fixed at some angle with respect to the scattering volume, which contains a large number of particles. Scattered light from each particle reaches the detector. Because the small particles are moving around randomly in the liquid, undergoing diffusive Brownian motion, the distance that the scattered waves travel to the detector varies as a function of time. Electromagnetic waves exhibit interference effects. Scattered waves can interfere constructively or destructively, depending on the distances traveled to the detector. The decay times of the fluctuations are related to the diffusion constants and, therefore, the size of the particles. The decay times of these fluctuations may be determined either in the frequency domain (with a spectrum analyzer) or in the time domain (with a correlator). The correlator is generally the most efficient means for this type of measurement.

Preparation of ABS-*g*-MA

Functionalization of ABS with MA was achieved by an emulsion polymerization method. In the preparation process, a polybutadiene (PB) polymer had to be synthesized first, and then, MA, AN, and St were polymerized on the PB particles. The PB latex used in this study was supplied by Jilin Chemical Industry Group Synthetic Resin Factory (Jilin, China). The recipe for the preparation of ABS-*g*-MA is given in Table II. The synthesis of ABS-*g*-MA was performed in a 2-L glass reactor under nitrogen at 80°C. First, the water, PB, initiator, and sodium dodecyl sulfate (SDS) were added to the glass reactor and stirred for 5 min under nitrogen, and then, the MA solution was added to the glass reactor and stirred for 10 min; finally, the St/AN (75/25) mixture was

TABLE II
Recipe of ABS-*g*-MA (1%)

Ingredient	Amount (g)
Water	1000
St	175.5
AN	58.5
MA	6
PB	360
$K_2S_2O_8$	3.6
SDS	2.4

added by continuous feeding to the glass reactor over about 4 h. The polymers were isolated from the emulsion by coagulation and dried in a vacuum oven at 60°C for 24 h before they were used.

Reactive blending and molding procedures

The blending of PA-6 was carried out in a twin-screw extruder. The compositions of the PA-6/ABS and PA-6/ABS-*g*-MA blends were 85/15, 80/20, 75/25, and 70/30 (w/w). The temperatures along the extruder were 210, 220, 240, 240, 240, 240, and 240°C, and the rotation speed of the screw was 60 rpm. The melt stripes of the blends were cooled in a water bath and then palletized.

The PA-6/ABS and PA-6/ABS-*g*-MA blends were dried in a vacuum oven at 80°C for 24 h. Then, injection-molding was carried out to prepare Izod impact specimens and tensile specimens. The notch of the Izod impact specimens was milled in by a machine with a depth of 2.54 mm, an angle of 45°, and a notch radius of 0.25 mm.

Rheological properties

The torque measurements of the PA-6/ABS and PA-6/ABS-*g*-MA blends were performed on a Thermo Hakke mixer (Karlsruhe, Germany). The rotating speed was set at 50 rpm, and the temperature was set at 240°C.

Morphological properties

The microstructure of the PA-6/ABS and PA-6/ABS-*g*-MA blends was observed by transmission electron microscopy (TEM; JEM-2000 EX, Tokyo, Japan). Ultramicrotomed sections were obtained with a Leica ultramicrotome (Wetzlar, Germany) at −100°C and stained with an OsO_4 solution for 8 h before observation.

SEM (JSM-5600, Tokyo, Japan) was used to characterize the fracture surfaces of the PA-6/ABS and PA-6/ABS-*g*-MA blends.

Mechanical properties

The notched Izod impact strength of the PA-6 blends was measured by an XJU-22 Izod impact tester (Chengde, China) at 23°C according to ASTM D 256. The dimensions of the samples were 63.5 × 12.7 × 6 mm^3. All materials for tensile testing were injection-molded into dumbbell type specimens whose dimensions of the parallel part were 65 mm in length with a cross section of about 12.9 × 2.90 mm^2. The tensile tests were carried out with a Shimadzu AGS-H 5KN tensile tester (Kyoto, Japan) at a crosshead speed of 50 mm/min at room temperature according to ASTM D 638.

RESULTS AND DISCUSSION

Fourier transform infrared (FTIR) analysis

FTIR was used to analyze the grafting properties of MA during the preparation process of ABS-*g*-MA. The ABS-*g*-MA copolymer was dissolved in acetone, and the solution was ultracentrifuged at room temperature at 10000 rpm with a GL-21M ultracentrifuge. After 30 min, clear separation was achieved. The ungrafted SAN and/or SAN-*co*-MA were soluble in acetone, whereas the ABS and/or ABS-*g*-MA copolymer were insoluble. The insoluble part was concentrated in a white layer at the tube bottom, and the clear solution of the ungrafted polymer concentrated at the top of the tube.

Curves 1 and 4 in Figure 1 show the FTIR spectra of the ABS-*g*-MA and ABS copolymer, respectively. For a comparison, the peak at 1778 cm^{-1} was the strong characteristic absorption of MA in curve 1, which indicated that the MA monomer was introduced onto the ABS copolymer. The FTIR spectra of the insoluble fraction and the soluble fraction of ABS-*g*-MA copolymer extracted from acetone are shown in curves 2 and 3, respectively. Both curves show the characteristic absorption of MA at 1778 cm^{-1}; however, both are less strong than that of the ABS-*g*-MA copolymer (curve 1), which indi-

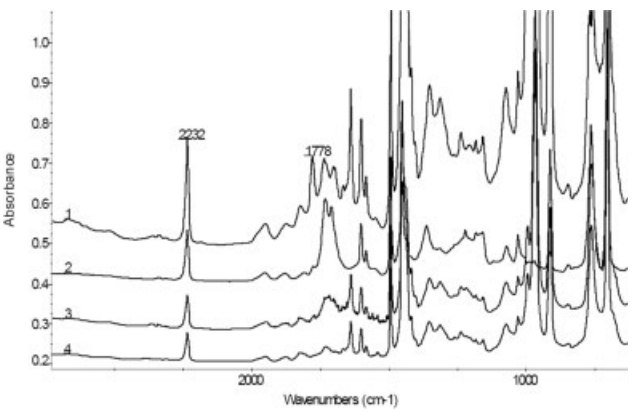

Figure 1 FTIR spectra of ABS and ABS-*g*-MA: (1) ABS-*g*-MA, (2) insoluble fraction of ABS-*g*-MA, (3) soluble fraction of ABS-*g*-MA, and (4) ABS.

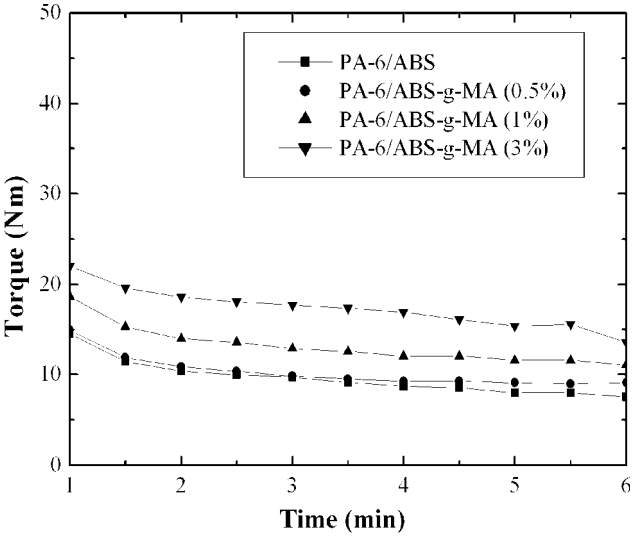

Figure 2 Evolution of torque with time in PA-6/ABS and PA-6/ABS-*g*-MA blends.

cated that some MA monomers grafted onto the PB particles or copolymerized with St and AN in the grafting shell and some MA monomers copolymerized with St and AN to form free SAN-*co*-MA copolymer.

Rheological properties

The evolution of torque versus time for the PA-6/ABS and PA-6/ABS-*g*-MA blends containing different MA contents in ABS-*g*-MA copolymer is shown in Figure 2. Compared to the PA-6/ABS-*g*-MA blend, PA-6/ABS had the lowest torque value because there was no chemical reaction between PA-6 and ABS. For the PA-6/ABS-*g*-MA blends, the torque value of these blends increased with increasing MA content in the ABS-*g*-MA copolymer. Figure 3 displays the relation between the actual temperature in the mixer and the mixing time for the PA-6 blends. The actual temperature in the mixer increased rapidly over a short time interval, and it reached 257°C for the PA-6/ABS blend, which was higher than the setting temperature of 240°C because of the viscous heating of the polymer. For the PA-6/ABS-*g*-MA blends, the temperature in the mixer got higher. This was due to the viscous heating of the highly viscous PA-6-*co*-ABS copolymer. Because the torque values of ABS and ABS-*g*-MA were almost the same, as shown in Table I, we concluded that the higher torque values and temperatures of the PA-6/ABS-*g*-MA blends compared to those of the PA-6/ABS blend were due to the reaction between the MA of ABS-*g*-MA and the amine groups of PA-6.

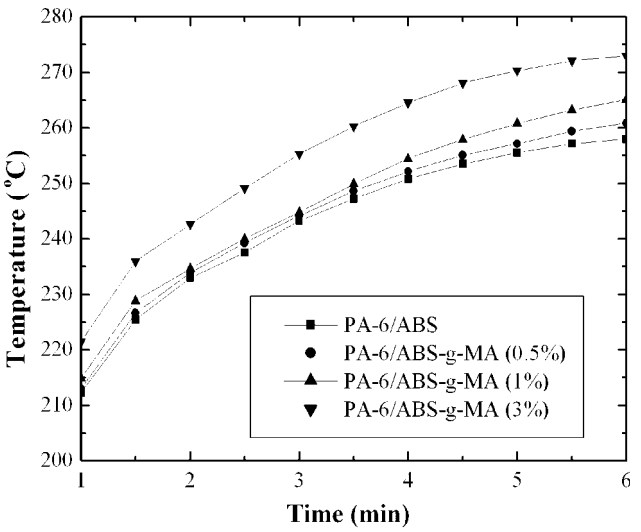

Figure 3 Evolution of temperature with time in PA-6/ABS and PA-6/ABS-*g*-MA blends.

Morphological properties

The dispersed phase morphology of the PA-6/ABS and PA-6/ABS-*g*-MA blends with MA contents ranging from 0.5 to 3% was investigated by TEM. The black particles stained by osmium tetroxide were PB in ABS, which indicated the morphology of the dispersed phase.

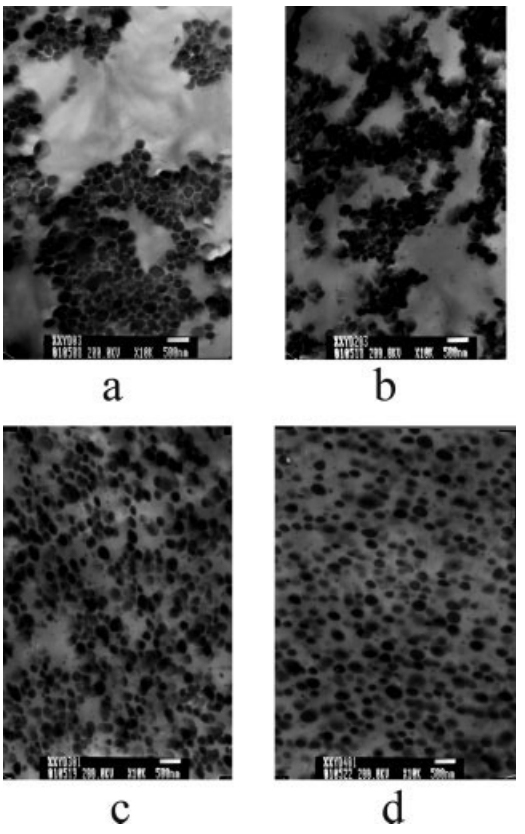

Figure 4 TEM photomicrographs of PA-6/ABS and PA-6/ABS-*g*-MA blends: (a) PA-6/ABS, (b) PA-6/ABS-*g*-MA (0.5%), (c) PA-6/ABS-*g*-MA (1%), and (d) PA-6/ABS-*g*-MA (3%).

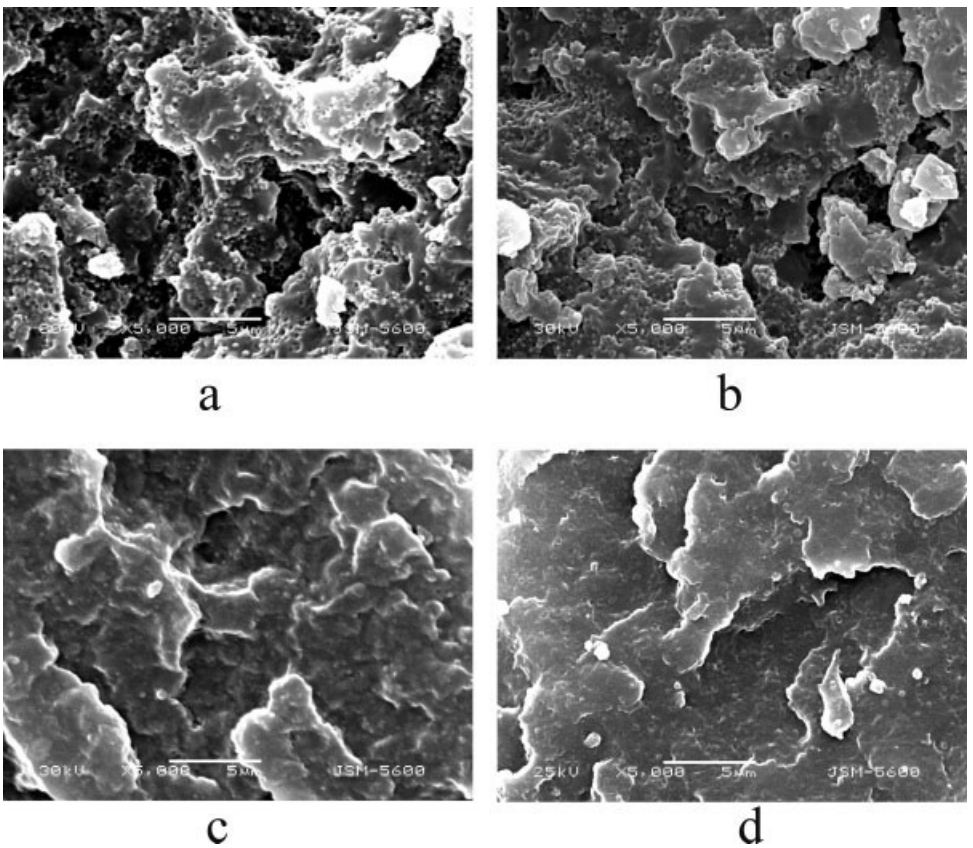

Figure 5 Freeze-fractured SEM micrographs of PA-6/ABS and PA-6/ABS-*g*-MA blends: (a) PA-6/ABS, (b) PA-6/ABS-*g*-MA (0.5%), (c) PA-6/ABS-*g*-MA (1%), and (d) PA-6/ABS-*g*-MA (3%).

Figure 4(a) presents the morphology of the PA-6/ABS blend. When the nonreactive ABS was mixed with PA-6, a very poor dispersion of ABS particles was obtained. In this blend, most of the ABS particles clustered together, which indicated the poor miscibility of PA-6 and ABS. Figure 4(b) displays the TEM micrographs of the PA-6/ABS-*g*-MA (0.5%) blend. The blend containing 0.5% MA in the ABS appeared to have little influence on the ABS particle dispersion in the matrix. Figure 4(c,d) displays the micrographs of the PA-6/ABS-*g*-MA (1%) and PA-6/ABS-*g*-MA (3%) blends. As shown, the coalescence of ABS particles was depressed, and the ABS particles dispersed in the PA-6 matrix uniformly. The better spatial distribution of ABS-*g*-MA identified the compatibilization effect of the PA-6-*co*-ABS copolymer.

Figure 5 shows the freeze-fractured SEM micrographs of the PA-6/ABS and PA-6/ABS-*g*-MA blends. As shown in Figure 5(a,b), ABS and ABS-*g*-MA (0.5%) clustered obviously in the PA-6 matrix, and the interface between PA-6 and the dispersed phase was clear, which showed poor interfacial adhesion between PA-6, ABS and ABS-*g*-MA (0.5%). As shown in Figure 5(c,d), ABS-*g*-MA (1%) and ABS-*g*-MA (3%) dispersed in the PA-6 matrix uniformly, and the interface between PA-6 and the dispersed phase was obscure, which showed that the interfacial adhesion between the two phases improved because of the compatibilization reactions between PA-6 and ABS-*g*-MA.

The possible chemical reactions that could occur between PA-6 and ABS-*g*-MA during melting processing shown in Scheme 1 were used to explain the morphology characteristics of these blends. A few articles[18,19] have reported that the predominant reaction in PA-6 and anhydride-functional polymers was between the anhydride and the amine end groups of

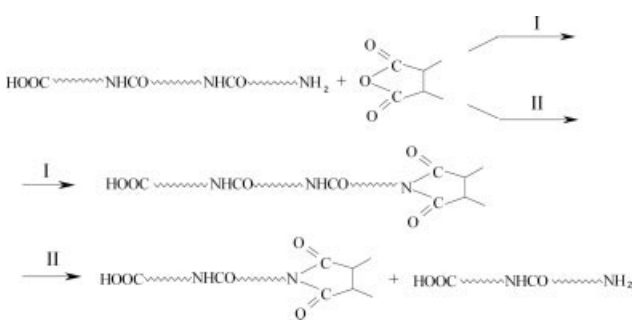

Scheme 1 Chemical reactions between PA-6 and MA functionalities.

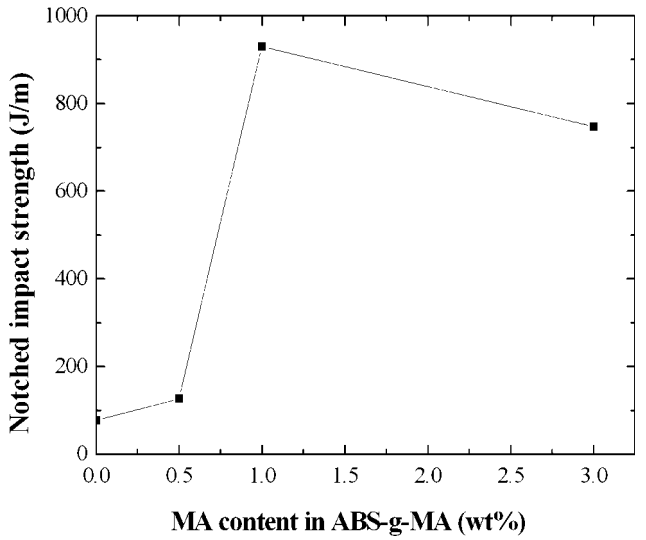

Figure 6 Notched impact strength of PA-6/ABS-*g*-MA (70/30) blends with different MA contents.

PA-6 (reaction I), which occurred very rapidly and resulted in the formation of imide. On the other hand, the anhydride could undergo interchange reactions with the amide linkages of PA-6 (reaction II), which formed an imide and a shorter polyamide chain. However, Legras et al.[33] and Tessier and Marechal[34] reported that the amine/anhydride reaction proceeded much faster than the amide/anhydride reaction in the systems.

Reactions I and II postulate the formation of the PA-6-*co*-ABS copolymers at the blend interface. The PA-6-*co*-ABS copolymer, acting as compatibilizer, could have increased the interfacial strengths. More important is that the coalescence of the disperse phase was suppressed through the interfacial stabilization effect because of the *in situ* reactions. These reactions resulted in a finer distribution of the disperse phase and response for the better morphological properties of the PA-6/ABS-*g*-MA blends.

Mechanical properties

The effect of MA content in ABS-*g*-MA on Izod impact strength of the PA-6/ABS-*g*-MA blends is shown in Figure 6. The PA-6/ABS blend still behaved as a brittle material because of the incompatibility of PA-6 and ABS. The incorporation of 0.5 wt % MA in ABS-*g*-MA generated no significant improvement in toughness; however, when the content of MA in ABS-*g*-MA increased to 1 wt %, the blends were supertough (>900 J/m). Because of the formation of PA-6-*co*-ABS, which acted as a compatibilizer, the ABS dispersed in the PA-6 matrix uniformly, and the PA-6/ABS-*g*-MA blends had a higher notched impact strength. With the increase of MA content in the ABS-*g*-MA copolymer, however, the notched impact strength of the PA-6/ABS-*g*-MA (3%) blend decreased slightly. Small amounts of MA (1%) in the ABS-*g*-MA copolymer appeared sufficient to improve the impact properties.

Figure 7 shows the effect of rubber content on the notched impact strength of the PA-6/ABS and PA-6/ABS-*g*-MA blends. The impact strength of the PA-6/ABS-*g*-MA (1 and 3%) blends increased with the ABS-*g*-MA content, whereas the impact strength of the PA-6/ABS-*g*-MA (0.5%) blend was close to that of the blends with no compatibilizer added because of the poor dispersion of ABS-*g*-MA (0.5%) in the PA-6 matrix. The PA-6/ABS-*g*-MA (1%) blend achieved the highest notched impact strength and displayed supertough behavior.

Table III summarizes the room-temperature tensile properties of the PA-6/ABS and PA-6/ABS-*g*-MA blends. As shown in Table III, the tensile strength and tensile modulus decreased significantly with increasing rubber content at a fixed MA amount. The decreases in tensile strength and modulus were due to the elastomeric nature of the PB rubber phase in ABS. On the other hand, the tensile strength and modulus increased to some degree with increasing MA content at the same rubber content because of the compatibilization reactions. The elongation at break had a relatively large standard deviation, which made it difficult to define clear trends. Many factors affect the elongation at break of a blend, including impurities, defects, and testing rate, in addition to intrinsic structure and morphology. Compared to the PA-6/ABS blends, the PA-6/ABS-*g*-MA blends had higher elongation at break values at the same disperse phase content.

Figure 8 shows the effect of temperature on the Izod impact strength of the PA-6/ABS and PA-6/

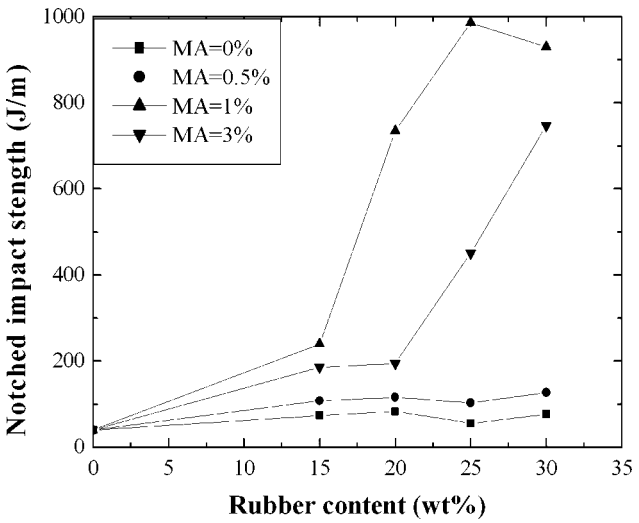

Figure 7 Notched impact strength of PA-6/ABS-*g*-MA blends with different rubber contents.

TABLE III
Room-Temperature Mechanical Properties of PA-6/ABS and PA-6/ABS-*g*-MA Blends

MA (wt %)	Rubber (wt %)	Izod impact strength at room temperature (J/m)	Yield stress (MPa)	Elongation at break (%)	Modulus (MPa)
0	15	74 ± 5	45.2 ± 0.4	216 ± 35	886.9 ± 21
0	20	83 ± 7	44.9 ± 0.3	169 ± 28	846.1 ± 17
0	25	56 ± 4	44.1 ± 0.3	250 ± 46	843.9 ± 19
0	30	77 ± 8	40.1 ± 0.4	156 ± 17	739.6 ± 9
0.5	15	108 ± 18	54.2 ± 0.5	220 ± 56	1085.9 ± 27
0.5	20	103 ± 14	51.1 ± 0.4	267 ± 46	1024.2 ± 35
0.5	25	116 ± 15	42.3 ± 0.5	366 ± 35	905.7 ± 18
0.5	30	127 ± 12	41.8 ± 0.5	293 ± 24	867.5 ± 22
1	15	240 ± 25	45.2 ± 0.6	199 ± 19	946.2 ± 31
1	20	735 ± 54	44.4 ± 0.4	185 ± 16	896.5 ± 25
1	25	986 ± 67	42.0 ± 0.5	272 ± 32	842.2 ± 17
1	30	930 ± 46	42.1 ± 0.5	210 ± 18	846.7 ± 21
3	15	186 ± 27	44.8 ± 0.5	229 ± 31	928.8 ± 25
3	20	194 ± 41	44.7 ± 0.7	243 ± 24	894.2 ± 18
3	25	451 ± 37	43.1 ± 0.6	253 ± 12	790.4 ± 20
3	30	747 ± 52	42.6 ± 0.6	166 ± 27	788.8 ± 24

ABS-*g*-MA blends containing various amounts of MA in the ABS-*g*-MA blends. The brittle–ductile transition temperature of PA-6/ABS blend was approximately 50°C, which was near the T_g of PA-6. With the introduction of MA into ABS, the brittle–ductile transition temperature of PA-6/ABS shifted to a lower temperature. The PA-6/ABS-*g*-MA (0.5%) blend fractured in ductile mode when the temperature was higher than 40°C. When the MA content increased to 1 and 3%, the brittle–ductile transition temperature decreased to 0°C.

Fracture mechanism

Figure 9 shows the fracture micrographs of the PA-6/ABS and PA-6/ABS-*g*-MA blends. The fracture surface of the PA-6/ABS blend is shown in Figure 9(a). It revealed the typical characteristics of brittle failure, a relatively flat smooth surface without any sign of deformation, and very limited stress whitening could be seen on the notch tip. The clear evidence of failure at the PA-6/ABS interface stemmed from the lack of adhesion between these phases. As for the PA-6/ABS-*g*-MA (0.5%) blend, shown in Figure 9(b), the PA-6-*co*-ABS compatibilizer was not sufficient to improve the interfacial adhesion. Therefore, its micrograph was comparable to the fracture micrograph of the PA-6/ABS blend. Figure 9(c,d) shows the fracture surfaces of the PA-6/ABS-*g*-MA (1%) and PA-6/ABS-*g*-MA (3%) blends, respectively. A great scale of stress whitening could be seen around the fracture surface, which is typical for a ductile fracture. There appeared to be a significant degree of plastic deformation of the matrix. The corresponding plastic deformation was high and effectively dissipated the fracture energy, which resulted in a highly improved impact strength at room temperature. Therefore, the shear yielding of the PA-6 matrix was the major toughening mechanism.

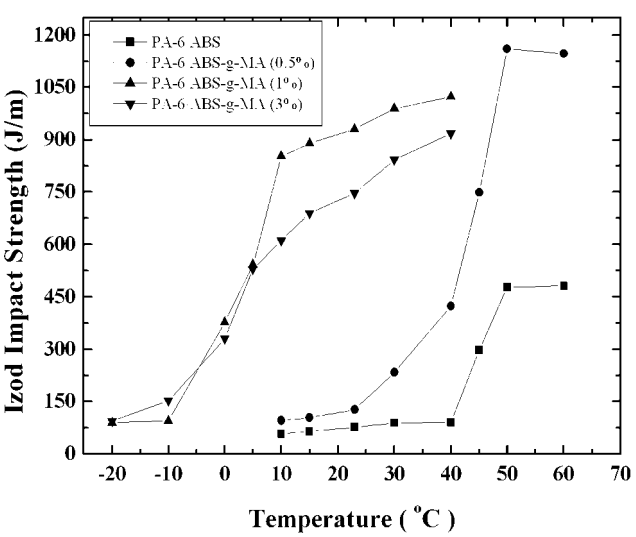

Figure 8 Effect of temperature on the Izod impact strength of PA-6/ABS and PA-6/ABS-*g*-MA blends.

CONCLUSIONS

A set of ABS-*g*-MA particles containing various amounts of anhydride groups were prepared by an emulsion polymerization processes. The ABS-*g*-MA particles were used as impact modifiers for PA-6. The FTIR results identify that MA was grafted onto the ABS.

Rheological testing showed that the torque value and temperature of these blends increased with MA content in the ABS-*g*-MA copolymer, which identified the reactions between MA of ABS-*g*-MA and the amine groups of PA-6.

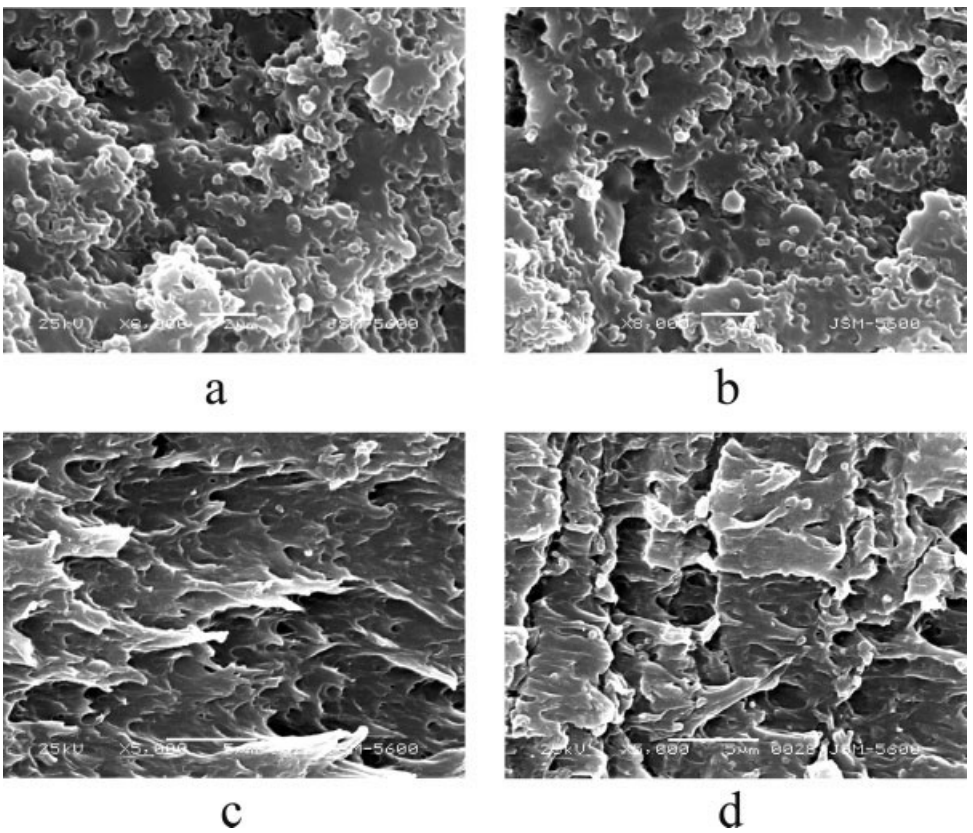

Figure 9 Micrographs of the fracture surfaces of PA-6/ABS and PA-6/ABS-*g*-MA blends (the fractures run from left to right): (a) PA-6/ABS, (b) PA-6/ABS-*g*-MA (0.5%), (c) PA-6/ABS-*g*-MA (1%), and (d) PA-6/ABS-*g*-MA (3%).

Morphological observation showed that when the nonreactive ABS particles were mixed with PA-6, a poor dispersion of ABS was obtained because of low interfacial adhesion between PA-6 and ABS. On the other hand, the PA-6/ABS-*g*-MA blends displayed a fine morphology. In these blends, two compatibilization reactions could have taken place: (1) a reaction between MA of ABS-*g*-MA and the amine groups of PA-6 and (2) a reaction between MA of ABS-*g*-MA and the amide groups of PA-6.

Mechanical tests showed that the presence of only a small amount of MA (1 wt %) within the disperse phase was sufficient to induce a pronounced improvement in the impact properties of the PA-6 blends. Moreover, the addition of MA in the blends decreased the brittle–ductile transition temperature of the PA-6 blends from 50 to 0°C.

SEM was used to study the toughening mechanisms of the PA-6 blends, and the results show that the shear yielding of PA-6 was the major toughening mechanism.

References

1. Utracki, L. A. Polymer Blends Handbook; Kluwer Academic Publishers: Dordrecht, Netherlands; 2002.
2. Kudva, R. A.; Keskkula, H.; Paul, D. R. Polymer 2000, 41, 225.
3. Oshinski, A. J.; Keskkula, H.; Paul, D. R. Polymer 1992, 33, 268.
4. Oshinski, A. J.; Keskkula, H.; Paul, D. R. Polymer 1992, 33, 284.
5. Dijkstra, K.; Terlaak, J.; Gaymans, R. J. Polymer 1994, 35, 315.
6. Dijkstra, K.; Gaymans, R. J. Polym Commun 1993, 34, 3313.
7. Takeda, Y.; Paul, D. R. J Polym Sci Part B: Polym Phys 1992, 30, 1273.
8. Modic, M. J.; Pottick, L. A. Polym Eng Sci 1993, 33, 819.
9. Borggreve, R. J. M.; Gaymans, R. J.; Schuijer, J.; Ingen Housz, J. F. Polymer 1987, 28, 1489.
10. Borggreve, R. J. M.; Gaymans, R. J.; Schuijer, J. Polymer 1989, 30, 63.
11. Lu, M.; Keskkula, H.; Paul, D. R. Polymer 1993, 34, 1874.
12. Lu, M.; Keskkula, H.; Paul, D. R. Polym Eng Sci 1994, 34, 33.
13. Lu, M.; Keskkula, H.; Paul, D. R. J Appl Polym Sci 1996, 59, 1467.
14. Paul, D. R.; Bucknall, C. B. Polymer Blends; Wiley: New York, 2000.
15. Lai, S. M.; Liao, Y. C.; Chen, T. W. Polym Eng Sci 2005, 45, 1461.
16. Majumdar, B.; Paul, D. R.; Oshinski, A. J. Polymer 1997, 38, 1787.
17. Huang, J. J.; Keskkula, H.; Paul, D. R. Polymer 2004, 45, 4203.
18. Kudva, R. A.; Keskkula, H.; Paul, D. R. Polymer 2000, 41, 239.
19. Yu, Z. Z.; Lei, M.; Ou, Y. C.; Hu, G. H. J Polym Sci Part B: Polym Phys 1999, 37, 2664.
20. Kudva, R. A.; Keskkula, H.; Paul, D. R. Polymer 1999, 40, 6003.
21. Majumdar, B.; Keskkula, H.; Paul, D. R. Polymer 1994, 35, 5453.
22. Majumdar, B.; Keskkula, H.; Paul, D. R. Polymer 1994, 35, 5468.
23. Majumdar, B.; Keskkula, H.; Paul, D. R.; Harvey, N. G. Polymer 1994, 35, 4263.

24. Sun, S. L.; Tan, Z. Y.; Xu, X. F.; Zhou, C.; Ao, Y. H.; Zhang, H. X. J Polym Sci Part B: Polym Phys 2005, 43, 2170.
25. Baer, M. U.S. Pat. 4,584,344(1986).
26. Lavengood, R. E.; Padwa, A. R.; Harris, A. F. U.S. Pat. 4,713,415 (1987).
27. Lavengood, R. E.; Patel, R.; Padwa, A. R. U.S. Pat. 4,777,211 (1988).
28. Majumdar, B.; Keskkula, H.; Paul, D. R. Polymer 1994, 35, 3164.
29. Kim, B. K.; Lee, Y. M.; Jeong, H. M. Polymer 1993, 34, 2075.
30. Misra, A.; Sawhney, G.; Kumar, R. A. J Appl Polym Sci 1993, 50, 1179.
31. Kudva, R. A.; Keskkula, H.; Paul, D. R. Polymer 1998, 39, 2447.
32. Araujo, E. M.; Hage, E., Jr.; Carvalho, A. J. F. J Appl Polym Sci 2003, 87, 842.
33. Marechal, P.; Coppens, G.; Legras, R.; Dekonincd, R. J Polym Sci Part A: Polym Chem 1997, 35, 901.
34. Tessier, M.; Marechal, E. J Polym Sci Part A: Polym Chem 1988, 26, 2785.